ISIJ International, Vol. 43 (2003), No. 7, pp. 1030–1035

# Hot Rolling of Light Gauge Steel Strip

P. C. ZAMBRANO, A. L. DELGADO, M. P. GUERRERO-MATA, R. COLÁS and L. A. LEDUC[1)]

Facultad de Ingeniería Mecánica y Eléctrica, Universidad Autónoma de Nuevo León, A.P. 149-F, 66451 San Nicolás de los Garza, N.L., México. 1) División Aceros Planos, Hylsa, S.A. de C.V., A.P. 996, 64000 Monterrey, N.L., México.

(*Received on January 25, 2002; accepted in final form on January 17, 2003*)

Production of hot rolled thin gauge steel strip in a compact six-stand mill was studied by means of mathematical modelling and on site measurements. Data obtained during processing low carbon steel strip ranging from 1.06 to 2.68 mm in final outgoing thickness included speeds, reductions and separation forces at each of the six stands. The mean flow stress during rolling was calculated from the rolling loads, assuming adhesive conditions within the roll-gap, and by means of a mathematical model that accounts for strain hardening and the occurrence of various dynamic restoration phenomena during deformation. It was found that the values of the mean flow stress values, independently of the way they were obtained, varied as a function of both, strain rate and temperature, being possible to derive a unique formulation to describe their behaviour.

KEY WORDS: hot rolling; thin gauge strip; flow stress; recrystallization.

## 1. Introduction

Steel strip of gauges thinner than 2 mm is normally produced by hot and cold rolling, a route that includes processes such as pickling, annealing and tempering. Cold rolling allows for the production of strips with narrow dimensional tolerances, tempering can be used to modify the surface roughness and appearance.[1–3)] Strips that have only been subjected to hot rolling are not used when surface quality and aspect are important, but there are applications in which thin gauged hot rolled strip can be a viable economical alternative to cold rolled strip.[4)]

During hot rolling, as in any other process conducted a temperatures above half of the melting temperature of the alloy, different dynamic restoration mechanisms occur. The material strengthens by deformation, and softens either by elimination or ordering of punctual or lineal defects (recovery), or by the reconstruction of the whole microstructure by the sweeping of high angle boundaries (recrystallization), when temperature, strain and time are high enough. The structure produced by deformation is not stable, as it may recrystallize in a static manner during the time available between passes. Moreover, the grains will grow once recrystallization has been achieved.[5–7)]

The above mentioned mechanisms affect the way microstructure changes, altering the strength of the material. Modern rolling practices require and rely on the prediction of this strength as the separation forces can be used to control the thickness and shape of the strip.[3)] Mathematical modelling is used to predict the thermal and microstructural evolution that takes place during rolling,[7–9)] and, with such information, the strength of the material can be calculated.[10–12)]

The aim of this work is to present the results found in a series of rolling trials carried out in an industrial mill producing thin gauge steel strip. Data related with the rolling procedure were obtained on line, and was complemented by modelling the process.

## 2. Rolling Trials

**Figure 1** shows an schematic diagram of the rolling mill in which the material was processed. Thin slab 50 mm in thickness is fed into the mill after being homogenized in a continuous furnace.[4,13,14)] The high temperature primary oxide formed on the steel slab is removed by a double header descaler prior to its deformation, the temperature during rolling can be regulated by interstand cooling headers. An air fan is located at the exit side of the mill to push down the strip and avoid aerodynamic problems arising by the combination of thin, light weight strip moving at speeds above 10 m/sec. The nominal diameter of the work rolls is of 790 mm for stands F1 to F3 and of 500 mm for stands F4 to F6.

**Table 1** shows the outgoing thickness and width as well as the chemical composition of the strips produced. **Table 2** resumes the data obtained from these trials. **Figure 2** shows the reduction imparted per pass to produce the strips of different thicknesses. **Figure 3** shows the speed at each pass as a function of exit thickness, the broken line corresponds to the nominal outgoing speed of the strips as a function of thickness.

## 3. Modelling

Modelling hot rolling requires computing the thermal evolution of the deforming stock, since the rate at which the microstructure evolves, and the flow stress of the material

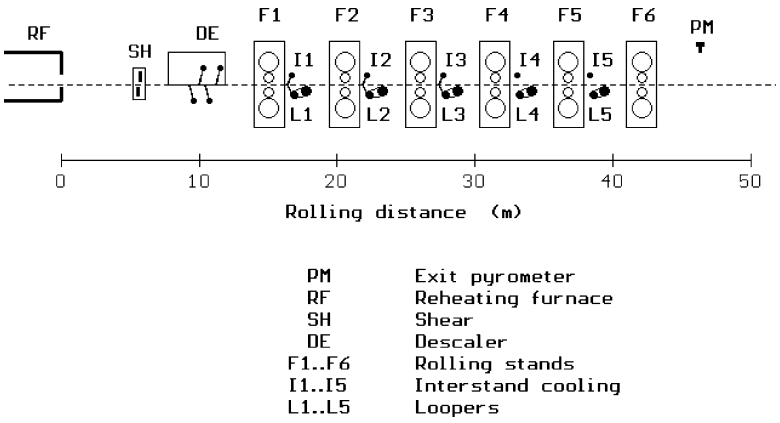


**Fig. 1.** Schematic diagram of the six-stand continuous rolling mill.

**Table 1.** Thickness, width and chemical composition (wt%) of the strips produced.

| Strip | Thickness (mm) | Width (mm) | C | Mn | P | S | Si | Al | Nb | N |
|---|---|---|---|---|---|---|---|---|---|---|
| **A** | 2.69 | 1,206 | 0.054 | 0.199 | 0.01 | 0.008 | 0.015 | 0.033 | 0.004 | 0.0043 |
| **B** | 1.92 | 1,206 | 0.050 | 0.199 | 0.01 | 0.007 | 0.015 | 0.031 | 0.006 | 0.0057 |
| **C** | 1.06 | 1,206 | 0.053 | 0.191 | 0.01 | 0.007 | 0.011 | 0.038 | 0.006 | 0.0062 |

**Table 2.** Summary of measured rolling parameters.

| | F1 | F2 | F3 | F4 | F5 | F6 |
|---|---|---|---|---|---|---|
| Strip **A** | | | | | | |
| Thickness (mm) | 24.34 | 13.52 | 7.16 | 4.76 | 3.45 | 2.69 |
| Speed (m/sec) | 0.6 | 1.1 | 2.0 | 3.2 | 4.4 | 5.8 |
| Reduction (%) | 51.3 | 44.5 | 47.0 | 33.5 | 27.5 | 22.0 |
| Force (MN) | 17.54 | 14.71 | 16.81 | 10.22 | 8.35 | 7.80 |
| Strip **B** | | | | | | |
| Thickness (mm) | 19.47 | 10.46 | 5.54 | 3.54 | 2.49 | 1.92 |
| Speed (m/sec) | 0.8 | 1.4 | 2.7 | 4.4 | 6.3 | 8.3 |
| Reduction (%) | 61.1 | 46.3 | 47.0 | 36.1 | 29.7 | 22.9 |
| Force (MN) | 19.72 | 15.48 | 16.26 | 10.96 | 10.16 | 9.36 |
| Strip **C** | | | | | | |
| Thickness (mm) | 16.94 | 7.41 | 3.32 | 1.95 | 1.36 | 1.06 |
| Speed (m/sec) | 0.7 | 1.5 | 3.4 | 6.0 | 9.0 | 12.0 |
| Reduction (%) | 66.1 | 57.7 | 53.6 | 41.3 | 30.3 | 22.1 |
| Force (MN) | 22.92 | 20.40 | 21.64 | 12.92 | 11.35 | 10.55 |

depends on the strain rate and temperature at which deformation is carried out.[7] The phenomena taken into account to describe thermal changes during this process are radiation and conduction to the surrounding media, conduction to the work rolls, forced convection and boiling of water used for descaling and interstand cooling, adiabatic heating produced during deformation and heat conduction within the stock. The finite difference model described elsewhere[9,14–17] is used in this work, the cross-sectional area of the strip is divided into small cells of equal size to approximate the equations for conduction. The model takes advantage of symmetry, so computations are carried out in only one quadrant after assuming equal condition on top and bottom and lateral surfaces. The general discussion on the thermal portion of the model, and the mathematical expressions used to compute the evolution can be found elsewhere.[9,14–17]

The procedure used to determine microstructural evolution evaluates whether or not dynamic recrystallization was achieved during a given pass depending on rolling conditions such as temperature, strain rate, reduction, *etc.* If the critical strain was surpassed, the dynamically recrystallized

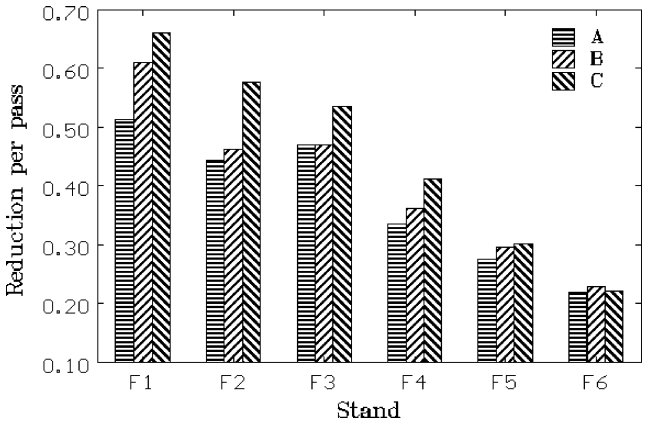


**Fig. 2.** Reduction per pass imparted to the different strips.

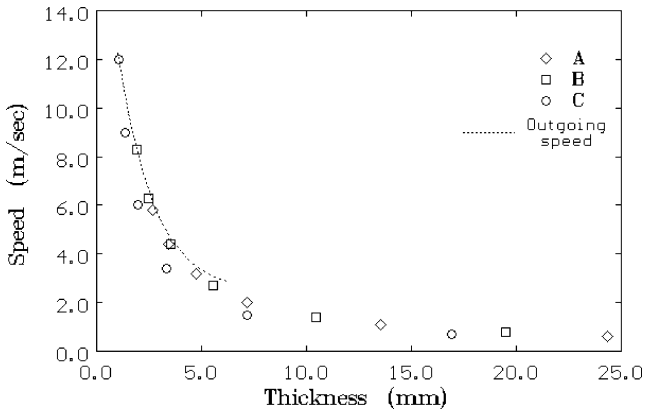


**Fig. 3.** Variation of speed as a function of the outgoing thickness in each pass. The nominal variation of speed as a function of the final thickness is plotted as a broken line.

fraction and the corresponding grain size are calculated, allowing for metadynamic recrystallization during the interpass time. If dynamic recrystallization did not take place, the kinetics equations for static restoration during the interpass time are used. The algorithm allows for strain accumulation between passes and for grain growth once recrystallization has been completed.[17–19]

The rolling force is calculated by integrating the variation of the flow stress as a function of strain that results from the rolling conditions within a given pass. The model computes the contribution from strain hardening and dynamic recovery and recrystallization, the later when the re-

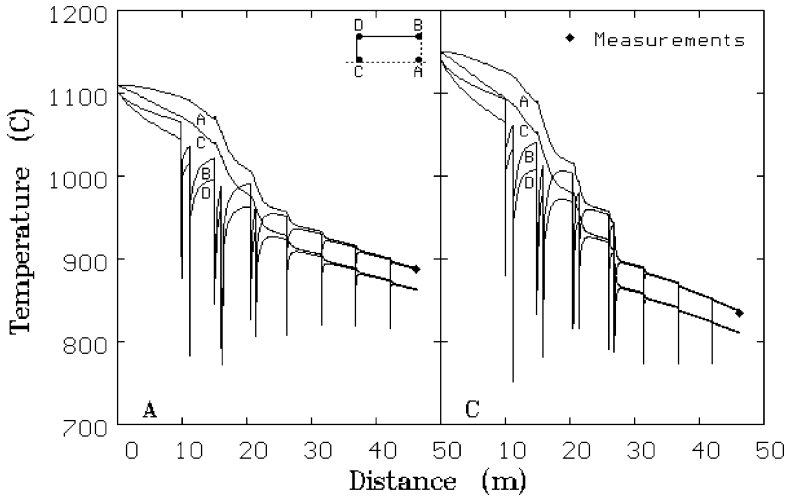


**Fig. 4.** Thermal evolution predicted by the model for the production of strips identified as A and C.

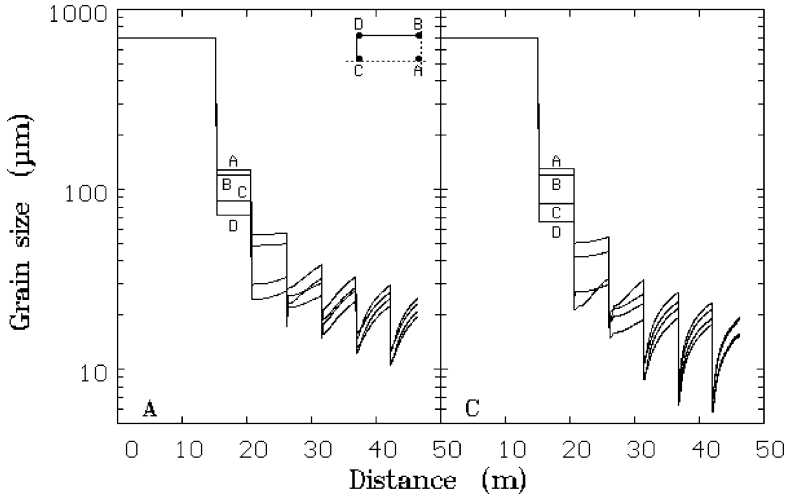


**Fig. 5.** Microstructural evolution predicted by the model for strips identified as A and C.

duction is high enough. The activation energy used depends on the chemical composition of the material.[12,17–19)]

## 4. Results

**Figure 4** shows the thermal evolution computed by the model for the strips identified as A and C. Each of the four curves represent one of the points indicated in the inserted diagram that represents one quadrant of the cross-sectional area. The temperatures recorded by the pyrometer located at the exit side of the mill, see Fig. 1, are indicated in both diagrams. Variation of the microstructure predicted by the model for these strips is shown in **Fig. 5**. The correlation between the temperatures registered during production of strips of different qualities and thickness and the values predicted by the mathematical model is shown in **Fig. 6**. An attempt to measure the temperatures on the strip at the roll gap, or close to it, was made with an infrared recorder,[20)] but as the data were considered unrealistic the temperatures predicted by the model were used in the analysis.

**Figure 7** shows the flow curves for the steel at each of the six stands. These curves were computed by means of the model described elsewhere[12)] using the average temperature value during rolling, see Fig. 4, and the average grain size before the pass, see Fig. 5. The activation energy used was computed from the chemical composition of the steel, Table 1.

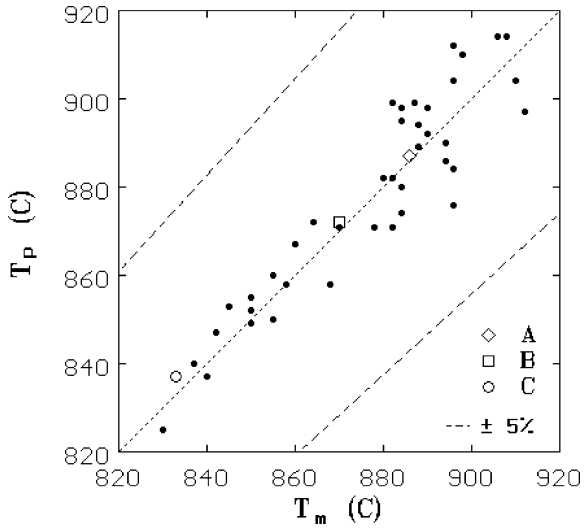


**Fig. 6.** Correlation between the temperatures measured ($T_m$) and predicted by the model ($T_p$). The broken lines correspond to a ±5% difference.

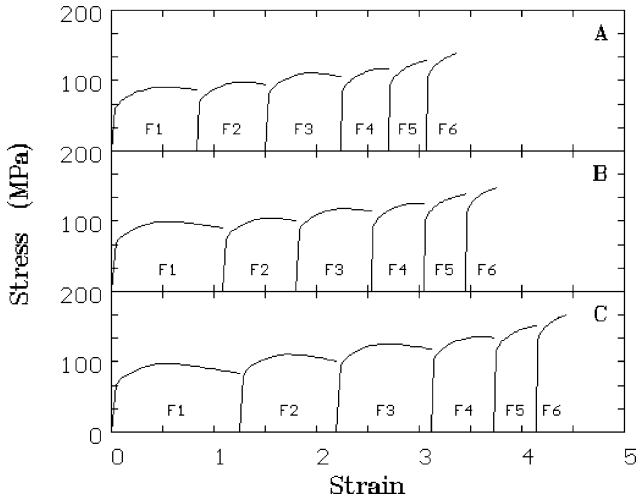


**Fig. 7.** Flow curves computed for the different strips.

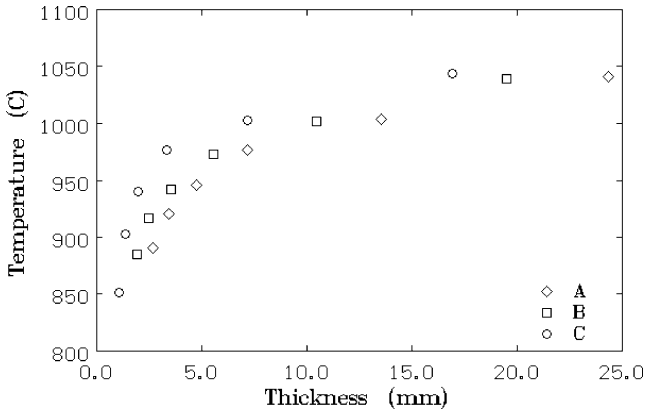


**Fig. 8.** Variation of the rolling temperature as a function of the outgoing thickness in each pass.

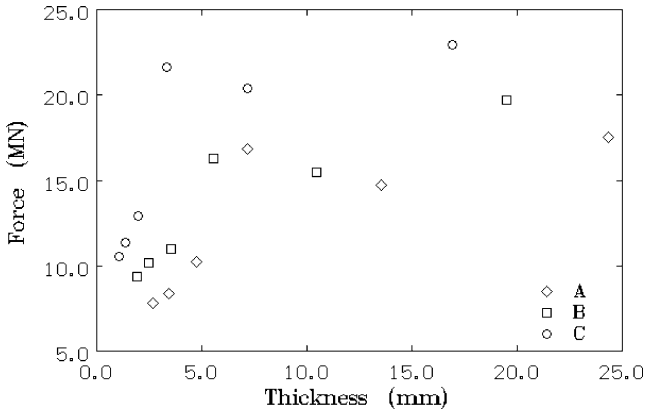


**Fig. 9.** Variation of the rolling forces as a function of the outgoing thickness in each pass.

**Figure 8** shows the variation of the average rolling temperature, computed by the mathematical model, as a function of the outgoing pass thickness, where it is worth noticing that all the data fall within the same scatter band. **Figure 9** shows the variation of the separation forces recorded during actual production as a function of the outgoing thickness in each pass. Two sets of data can be identified, one corresponding to the first three stands (above 15 MN) and those registered by the loads cells from the last three stands (below 15 MN), the difference between these

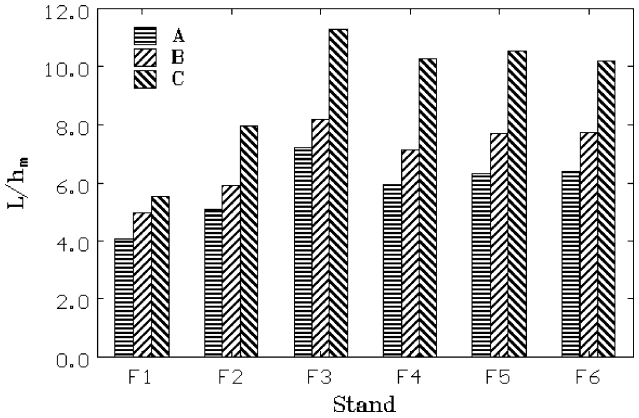


**Fig. 10.** Changes in the reduction geometry of the different strips.

sets is due to the difference in diameter of the work rolls used in the stands, that results in change of the projected length of the arc of contact ($L$)[1–3]:

$$L=(R'\Delta h)^{1/2} \quad \text{.....(1)}$$

where $R'$ is the deformed radius of the work roll and $\Delta h$ is the reduction of height (draft) in a given pass. **Figure 10** shows the variation of the reduction geometry, expressed as the ratio of $L$ over the mean rolling thickness ($h_m$), of the different strips. It is worth noticing that such ratio is always above one, which indicates the validity in neglecting strain heterogeneities while modelling,[21] and that this ratio remains more or less constant in the last three stands for each final thickness. The mean rolling thickness is expressed as:

$$h_m=(h_i h_o)^{1/2} \quad \text{.....(2)}$$

where $h_i$ and $h_o$ are the ingoing and outgoing thicknesses at each stand.

## 5. Discussion

The average flow stress of the material at each rolling pass can be computed from the rolling loads, that were recorded during production, assuming adhesive frictional conditions at the roll-gap:

$$\bar{\sigma}_r=\frac{P}{1.15wLQ_p} \quad \text{.....(3)}$$

where $\bar{\sigma}_r$ is the average stress, $P$ is the rolling load, $w$ the width of the strip, $L$ the projected arc of contact, the 1.15 factor allows for conversion from plane strain compression conditions and $Q_p$ is a geometric term.[22,23] The values of this average value of stress can be plotted as a function of the reduction imparted at each pass, **Fig. 11**, where it can be seen that all the data fall within a single band, with the lower values of strength towards the higher reductions, but this effect is due to the fact that the magnitude of the reduction is reduced as the strip is being processed, Fig. 2, and its temperature increases, Fig. 8.

The average flow stress can also be computed by the integration of the stress–strain curves shown in Fig. 7. In such a case, the stress ($\bar{\sigma}_m$) can be calculated by:

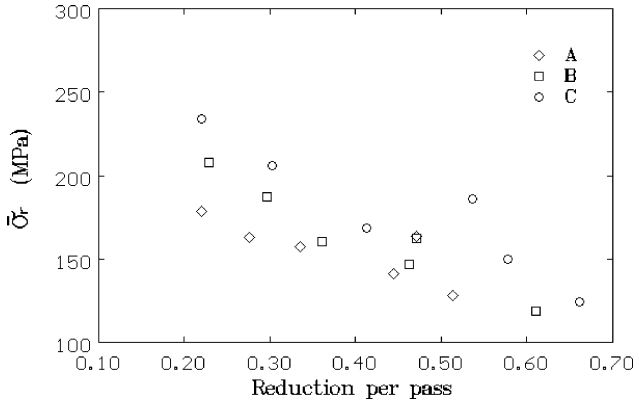


**Fig. 11.** Variation of the average value of stress computed from the rolling loads as a function of the reduction imparted.

**Table 3.** Summary of computed processing parameters.

| | F1 | F2 | F3 | F4 | F5 | F6 |
|---|---|---|---|---|---|---|
| Strip **A** | | | | | | |
| Temperature (C) | 1041 | 1004 | 977 | 946 | 921 | 891 |
| Grain size ($\mu$m) | 700 | 120 | 55 | 25 | 20 | 18 |
| $\dot{\varepsilon}$ (sec$^{-1}$) | 5.4 | 16.7 | 43.8 | 52.4 | 73.6 | 94.9 |
| $\bar{\sigma}_m$ (MPa) | 125 | 135 | 154 | 160 | 173 | 186 |
| $\bar{\sigma}_r$ (MPa) | 128 | 141 | 163 | 157 | 163 | 177 |
| Strip **B** | | | | | | |
| Temperature (C) | 1039 | 1002 | 973 | 942 | 917 | 885 |
| Grain size ($\mu$m) | 700 | 117 | 52 | 23 | 19 | 15 |
| $\dot{\varepsilon}$ (sec$^{-1}$) | 6.6 | 25.0 | 67.2 | 88.3 | 130.6 | 164.8 |
| $\bar{\sigma}_m$ (MPa) | 137 | 144 | 164 | 173 | 187 | 199 |
| $\bar{\sigma}_r$ (MPa) | 119 | 147 | 162 | 161 | 188 | 208 |
| Strip **C** | | | | | | |
| Temperature (C) | 1044 | 1003 | 977 | 940 | 903 | 851 |
| Grain size ($\mu$m) | 700 | 115 | 50 | 21 | 18 | 13 |
| $\dot{\varepsilon}$ (sec$^{-1}$) | 8.3 | 38.4 | 127.5 | 180.2 | 256.0 | 313.2 |
| $\bar{\sigma}_m$ (MPa) | 133 | 153 | 176 | 189 | 206 | 227 |
| $\bar{\sigma}_r$ (MPa) | 125 | 150 | 168 | 186 | 206 | 234 |

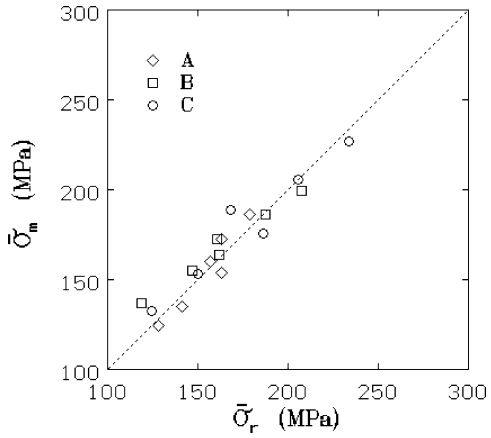


**Fig. 12.** Correlation between the mean stress values.

$$\bar{\sigma}_m = \frac{1}{\varepsilon_f - \varepsilon_o} \int_{\varepsilon_o}^{\varepsilon_f} \sigma d\varepsilon \quad \text{.....(4)}$$

where $\varepsilon_o$ and $\varepsilon_f$ correspond to the strain at the start and end of each pass. The values computed for both sorts of average stress ($\bar{\sigma}_r$ and $\bar{\sigma}_m$), together with the average values of temperature, grain size and strain rate, used to calculate them are shown in **Table 3**. **Figure 12** shows the agreement between $\bar{\sigma}_r$ and $\bar{\sigma}_m$.

The diagrams shown in Fig. 5 indicate that the microstructure is able to recrystallize during the time available between passes, and, in some cases, this period of time is high enough to exhibit grain growth, following a pattern well described before.[7,9,17–19,22] Such behaviour allows for computing the stress–strain curves shown in Fig. 7 without any previous accumulation of strain.

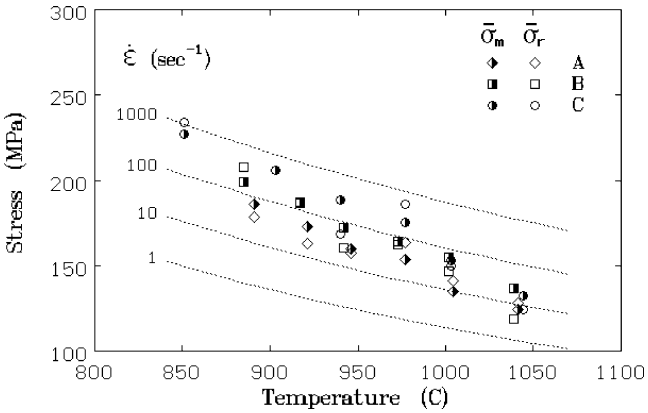


**Fig. 13.** Temperature dependence of the mean stress values.

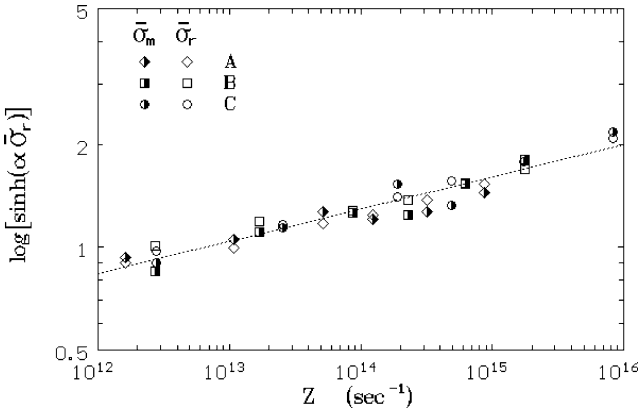


**Fig. 14.** Variation of the mean stress values with respect to the Zener–Hollomon parameter.

**Figure 13** shows the temperature dependence of either $\bar{\sigma}_r$ or $\bar{\sigma}_m$, computed by means of Eq. (3) or (4), respectively. It can be seen that the strength of the material increases as the temperature diminishes, and, although all the data, independently of the rolling reduction, fall within a single scatter band, it should be noticed that the average strain rate during the pass increased with the reduction in thickness, Table 3, therefore the dotted lines, that show different strain rate levels, were plotted in Fig. 13. **Figure 14** shows that the mean stress values can be related to a unique formulation based on the Zener–Hollomon parameter ($Z$). The value of the apparent activation energy for deformation was that computed from the chemical composition of the steel.[12]

## 6. Conclusions

A series of experimental trials were conducted in an industrial rolling mill to obtain information related to the production of hot rolled light gauge steel strip. The data gathered were compared with the results of a mathematical model developed to predict the behavior of carbon steel as it is being hot rolled.

It was found a good correlation between the temperatures

predicted by the model and those measured at the end of processing. The mean stress values computed from the rolling loads assuming adhesive frictional condition, and by the integration of the stress–strain curves obtained by using the average temperature and grain size agreed with each other. It was found that the mean stress value followed a unique formulation based in the Zener–Hollomon parameter.

**Acknowledgements**

The authors acknowledge the facilities given by Hylsa, S.A. de C.V., during this work. MPGM and RC thank the support provided by CONACYT and PAICYT-UANL.

## REFERENCES

1) W. Roberts: Cold Rolling of Steel, Marcell Dekker, Inc., New York, (1978).
2) W. Roberts: Flat Processing of Steel, Marcell Dekker, Inc., New York, (1982).
3) W. Ginzburg: Steel Rolling: Theory and Practice, Marcell Dekker, Inc., New York, (1989).
4) L. LeDuc-Lezama, M. Vazquez-del-Mercado and R. Gonzalez-de-la-Peña: *Iron Steel Eng.*, **23** (1997), No. 4, 27.
5) I. Tamura, C. Ouchi, T. Tanaka and H. Sekine: Thermomechanical Processing of High Strenght Low Alloy Steels, Butterworths, London, (1988).
6) H. J. McQueen and J. J. Jonas: Plastic Deformation of Metals, ed. by R. J. Arsenault, Academic Press, New York, (1975), 393.
7) C. M. Sellars: *Mater. Sci. Technol.*, **1** (1985), 325.
8) F. Hollander: Mathematical Models in Metallurgical Process Development, Iron Steel Inst. Sp. Pub. 123, Iron and Steel Institute, London, (1970), 46.
9) R. Colás: *Mater. Sci. Technol.*, **14** (1998), 388.
10) C. M. Sellars: *Czech. J. Phys.*, **B35** (1985), 239.
11) A. Laasraoui and J. J. Jonas: *Metall. Trans. A*, **22A** (1991), 1145.
12) R. Colás: *J. Mater. Process. Technol.*, **62** (1996), 180.
13) G. Flemming, W. Hennig, F. Hofmann, F.-P. Pleschiutschingg, D. Rosental and J. Schwellenbach: *Metall. Plant Technol. Int.*, **16** (1997), No. 3, 64.
14) L. A. Leduc-Lezama and J. Muñoz-Baca: 39th Mech. Worl. Steel Proc. Conf., Vol. 35, ISS-AIME, Warrendale, PA, (1997), 89.
15) R. Colás: *Mod. Sim. Mat. Sc. Eng.*, **3** (1995), 437.
16) R. Colás, L. Elizondo and L. A. Leduc: 2nd Int. Conf. Modelling of Metal Rolling Processes, eds. by J. H. Beynon, P. Ingham, H. Teichert and K. Watson, Institute of Materials, London, (1996), 12.
17) R. Colás: Advances in Hot Deformation Textures and Microstructures, eds. by J. J. Jonas, T. R. Bieler and K. J. Bowman, TMS-AIME, Warrendale, PA, (1994), 63.
18) M. Hinojosa, U. Ortiz, L. A. Leduc and R. Colás: Recrystallization '92, ed. by M. Fuentes and J. Gil Sevillano, *Mater. Sci. Forum*, **112–115** (1993), 323.
19) M. Hinojosa, U. Ortiz and R. Colás: Recrystallization '92, ed. by M. Fuentes and J. Gil Sevillano, *Mater. Sci. Forum*, **112–115** (1993), 467.
20) G. García-Gil and R. Colás: *Int. J. Mach. Tools Manuf.*, **40** (2000), 1977.
21) J. H. Beynon and C. M. Sellars: Modelling of Plastic Deformation and its Engineering Applications, eds. by S .I. Andersen, J. B. Bilde-Sørensen, N. Hansen, D. Juul Jensen, T. Leffers, H. Lilholt, T. Lorentzen, O. B. Pedersen and B. Ralph, Risø National Laboratory, Roskilde, (1992), 13.
22) C. M. Sellars: *Ironmaking Steelmaking*, **22** (1995), 459.